Published in final edited form as:

Clin Cancer Res. 2021 August 01; 27(15): 4245–4255. doi:10.1158/1078-0432.CCR-20-4450.

Standardized Uptake Value for ^{18}F-Fluorodeoxyglucose is a Marker of Inflammatory State and Immune Infiltrate in Cervical Cancer

John M Floberg[1,2], **Jin Zhang**[1], **Naoshad Muhammad**[1], **Todd A DeWees**[3], **Matthew Inkman**[1], **Kevin Chen**[4], **Alexander J Lin**[1], **Ramachandran Rashmi**[1], **Kay Jayachandran**[1], **Brian T Edelson**[5], **Barry A Siegel**[6,7], **Farrokh Dehdashti**[6,7], **Perry W Grigsby**[1,6,7], **Stephanie Markovina**[1,7], **Julie K Schwarz**[1,7,8]

[1]Department of Radiation Oncology, Washington University School of Medicine, St. Louis, MO

[2]Department of Human Oncology, University of Wisconsin School of Medicine and Public Health, Madison, WI

[3]Division of Biomedical Statistics and Informatics, Mayo Clinic, Phoenix, AZ

[4]Washington University School of Medicine, St. Louis, MO

[5]Department of Pathology and Immunology, Washington University School of Medicine, St. Louis, MO

[6]Mallinckrodt Institute of Radiology, Washington University School of Medicine, St. Louis, MO

[7]Alvin J. Siteman Cancer Center, Washington University School of Medicine, St. Louis, MO

[8]Department of Cell Biology and Physiology, Washington University School of Medicine, St. Louis, MO

Abstract

Purpose: Chemo-radiotherapy for locally advanced cervical cancer fails in over a third of patients. Biomarkers with therapeutic implications are therefore needed. We investigated the relationship between an established prognostic marker, maximum standardized uptake value (SUV_{max}) on ^{18}F-fluorodeoxyglucose positron emission tomography, and the inflammatory and immune state of cervical cancers.

Experimental Design: An SUV_{max} most prognostic for freedom from progression (FFP) was identified and compared to known prognostic clinical variables in a cohort of 318 patients treated with definitive radiation with prospectively collected clinical data. Gene set enrichment analysis (GSEA) and CIBERSORT of whole transcriptome data from 68 patients were used to identify biological pathways and immune cell subpopulations associated with high SUV_{max}. Immunohistochemistry using a tissue microarray (TMA, N=82) was used to validate the

Corresponding Author: Julie Schwarz, MD, PhD, **Address:** Department of Radiation Oncology; Washington University School of Medicine, 4511 Forest Park Avenue, Saint Louis, MO 63108, **Phone:** 314-273-0275, **FAX:** 314-747-5498, jschwarz@wustl.edu.

Conflicts of Interest: The authors declare no potential conflicts of interest.

CIBERSORT findings. The impact of macrophages on cervical cancer glucose metabolism was investigated in co-culture experiments.

Results: SUV_{max} <11.4 was most prognostic for FFP (p=0.001). The GSEA showed that high SUV_{max} is associated with increased gene expression of inflammatory pathways, including JAK/STAT3 signaling. CIBERSORT and CD68 staining of the TMA showed high SUV_{max} tumors are characterized by a monocyte-predominant immune infiltrate. Co-culture of cervical cancer cells with macrophages or macrophage-conditioned media altered glucose uptake, and IL-6 and JAK/STAT3 signaling contribute to this effect.

Conclusion: SUV_{max} is a prognostic marker in cervical cancer that is associated with activation of inflammatory pathways and tumor infiltration of myeloid-derived immune cells, particularly macrophages. Macrophages contribute to changes in cervical cancer glucose metabolism.

Keywords

Cervical cancer; Immune cells and the microenvironment; Imaging biomarkers; High-throughput sequencing; Positron emission tomography (PET); Radiation Oncology

INTRODUCTION

Despite significant advances in screening and prevention, cervical cancer remains a leading cause of cancer deaths in women worldwide (1). The standard treatment for locally advanced cervical cancer, definitive pelvic radiation therapy (RT) given with concurrent cisplatin chemotherapy, has not been improved upon for nearly twenty years, despite the fact that this therapy fails in approximately one third of patients (2–4). Treatments for recurrent and metastatic cervical cancer are limited, associated with significant morbidity, and rarely curative (5, 6). Therefore, innovative treatment strategies are needed.

A number of prognostic imaging markers have been developed for cervical cancer, including metrics derived from positron emission tomography with ^{18}F-fluorodeoxyglucose (FDG-PET) and magnetic resonance imaging (MRI) (7–11). We have previously demonstrated that persistent or progressive disease on post-treatment FDG-PET is a powerful negative prognostic marker, and that it is associated with PI3K/AKT pathway activation (8, 12). However, this is of limited value when making initial treatment decisions, thus a pre-treatment marker is desireable. Pre-treatment maximum standardized uptake value (SUV_{max}) of the primary tumor is particularly suited for this purpose. Other potentially more robust PET metrics have been proposed, but SUV_{max} is the most widely clinically reported, most widely studied, and we have previously reported its prognostic significance in cervical cancer patients (7). A deeper knowledge of primary tumor biology associated with a high SUV_{max} would further our understanding of how high risk cancers should be treated, and could transform FDG-PET signal from a prognostic marker to a marker predictive of response to specific therapies.

The purpose of this work was to identify targetable signaling pathways, genetic signatures, and immune cell populations enriched in cervical cancers with a high pre-treatment SUV_{max}. We established an SUV_{max} cutoff most prognostic for freedom from progression (FFP) in a cohort of cervical cancer patients treated with definitive RT using modern

techniques to identify high-risk cancers, confirming our prior work that established SUV_{max} as prognostic in a new cohort of patients (7). We used whole transcriptome RNA_{seq} data from a subcohort of patients to identify signaling pathways associated with high SUV_{max} using gene set enrichemnt analysis (GSEA). We likewise used the RNA_{seq} data to identify immune cell populations associated with high SUV_{max} using CIBERSORT, and confirmed these results using a tissue microarray (TMA). Finally, we performed benchtop studies to further explore the impact of macrophages on cervical cancer glucose metabolism and the signaling pathways identified in the GSEA.

MATERIAL AND METHODS

Patient Cohorts

1) SUV_{max} Cohort—All studies involving patient records and samples were conducted in accordance with the Declaration of Helsinki. A SUV_{max} cutoff with the most prognostic value was determined a cohort of patients with cervical cancer treated with definitive RT at our institution between 2006 and 2015. To be included, patients had to have completed the entire prescribed course of definitive-intent RT. FIGO stage I-IVa tumors (FIGO 2009 staging) and all histologic subtypes were allowed, patients with metastatic disease were excluded, all patients were >18 years old at the time of their diagnosis, and all patients underwent pretreatment FDG-PET/computed tomography (FDG-PET/CT) or FDG-PET/magnetic resonance imaging (FDG-PET/MRI). Details of our institutional practice for treating cervical cancer with RT have previously been reported (13). Briefly, patients were treated with external beam radiation therapy to the pelvis using intensity modulated radiation therapy, and to the para-aortic lymph nodes if they were involved. The primary cervical tumor was also treated with image guided brachytherapy. Nearly all (90.1%) patients were treated with concurrent chemotherapy. This cohort of patients was analyzed with institutional review board (IRB) approval with waiver of consent (IRB #201601052).

2) Whole Transcriptome RNA Sequencing Cohort—The second cohort of patients was used to identify overexpressed genes and pathways associated with high FDG uptake. This consisted of patients enrolled on a prospective tumor banking study with written informed consent (IRB #201105374). Overlap between this cohort and the SUV_{max} cohort are described in the results below and in Supplemental Figure 1S. Tumor samples with sufficient high-quality RNA for whole transcriptome sequencing (RNAseq), as defined by the criteria utilized for The Cancer Genome Atlas (TCGA), were included in this study (14). Tumors were not macro dissected and thus results are expected to include genes attributable to tumor and any infiltrating stromal or immune cells.

3) Tissue Microarray Immunohistochemistry Cohort—The third cohort of patients consisted of patients whose tumor samples were incorporated into a tissue microarray (TMA), and were interpretable for immunohistochemistry (IHC) analysis. Overlap between this cohort and the SUV_{max} cohort are also described in the results below and in Supplemental Figure 1S. This was also done with a waiver of consent from the IRB for access to tissue specimens and clinical data (IRB #201807063). Cohort 3 was also composed of patients treated with definitive RT.

PET/CT Imaging and Analysis

FDG-PET was performed as part of routine staging evaluation of patients with newly diagnosed cervical cancer according to our institution's imaging protocols, which have been developed to maximize visualization of cervical tumors (15). Briefly, patients were required to fast for at least 4 hours prior to FDG injection, and blood glucose levels were required to be less than 200 mg/dL at the time of tracer injection (5/331 patients had a blood glucose over 200 mg/dL). PET/CT images were acquired approximately 60 minutes after FDG injection. Images were acquired on 1 of 3 PET/CT scanners: Siemens Biograph 2 (n = 107), Siemens Biograph 40-HD (n = 187), and Siemens mCT (n = 32), and on one PET/MRI scanner (Siemens mMR, n = 5). All images were reconstructed using standard iterative reconstruction algorithms.

As part of routine clinical practice, the SUV_{max} of the primary cervical tumor was measured by determining the maximum single-voxel SUV within a volume of interest encompassing the primary tumor. A representative image of a large cervical tumor with an automatically generated metabolic tumor volume is shown in Supplemental Figure 2S. The SUV is defined as: SUV_{max} = (tissue radioactivity concentration (mCi/mL) x patient weight (g))/injected dose (mCi).

Statistical Analysis of Clinical Data

Given the significant overlap between the cohort of patients used in the SUV analysis and the cohort of patients used for the RNAseq analysis, a comparison was made between patients included only in the SUV analysis cohort and patients included in both cohorts using the Wilcoxon two-sample test and Fisher's exact test, as appropriate.

The optimal SUV_{max} for discriminating patients with good versus poor freedom from progression (FFP) was determined by outcome-oriented cutoff methodology utilizing an alpha-adjusted log-likelihood test (16). Once the optimal SUV_{max} was determined, the prognostic significance of this SUV_{max} for FFP, cancer-specific survival (CSS), and overall survival (OS) was evaluated with Kaplan-Meier/log-rank and Cox univariate and multivariate analysis. For FFP any recurrence was counted as an event and patients were censored at time of last follow-up. For CSS death from cervical cancer was counted as an event, and for OS death from any cause was counted as an event. In either case patients were censored at time of last follow-up or death.

A bootstrap Cox multivariate analysis was then performed to better illustrate the significance of SUV_{max} in the context of other known clinical prognostic markers. The bootstrap analysis was performed by taking 1000 random samplings from the first cohort of patients, such that each sampling was half the size of the total cohort. A Cox multivariate analysis was then run on each sampling. The variables included in this analysis were SUV_{max}, FIGO stage, lymph node involvement by FDG-PET (none, pelvic, para-aortic/supraclavicular), age, and histology (squamous vs. non-squamous).

Gene set enrichment analysis (GSEA)

We performed RNA_{seq} analysis on the patients in cohort 2. Specific details regarding this are included in the Supplemental Methods. The expressed genes were ranked according to fold-change between patients with high SUV_{max} (≥11.41) and low SUV_{max} (<11.41) values and included to perform GSEA analysis using default parameters (21). The H: hallmark gene sets (n=50) and the C2: curated gene sets (n=4,762) from the Molecular Signatures Database (MSigDB) were used to discover altered biological pathways between cervical cancer patients with an SUV_{max} above or below the cut-point established in the SUV_{max} analysis (21).

Cell-type abundance analysis

Using CIBERSORT, we estimated the relative abundances of hematopoietic cells in the patients from cohort 2 (22). For signature genes, we used the leukocyte gene signature matrix, LM22, which contains 547 genes that distinguish 22 human hematopoietic cell phenotypes, including seven T-cell types, naïve and memory B cells, plasma cells, natural killer (NK) cells and myeloid subsets. Relative fractions of B cells, CD4 T cells, CD8 T cells, neutrophils (M0, M1, and, M2), macrophages, monocytes, dendritic cells, and NK cells were compared between patients with high and low SUV_{max} using Student's *t*-test.

Prevalence of Immune Cell Populations in Cervical Tumors Using a Tumor Microarray

To evaluate the prevalence of various immune cells in human cervical tumors, we performed IHC for markers of macrophages and neutrophils on a TMA of human cervical cancer tumors. Details regarding this TMA have previously been published (23), and are outlined in more detail in the Supplemental Methods. Briefly, areas of cancer on formalin-fixed paraffin-embedded (FFPE) tumor specimens were identified and triplicate 1.5 mm cores were placed in a TMA. Sections 6 μm thick were then mounted onto polarized slides for IHC staining. Staining for macrophages was done on a Ventana automated stainer (Ventana Medical Systems). Staining was performed with anti-CD68 (0.4 μg/mL, monoclonal mouse, Ventana) and anti-CD163 (0.3 μg/mL, monoclonal mouse, Cell Marque). Neutrophil staining was performed manually, and slides were co-stained with CD66b (1:600, BD Biosciences) and neutrophil elastase (1:200, Novus).

Stained slides were digitally scanned and analyzed using the Aperio eSlide Manager platform (Leica Biosystems). Samples were considered either negative (≤1% of cells stained) or positive (>1% of cells) for all IHC stains used. Categorizing immune infiltrate as high versus low has previously been described, including for CD68 (24–26). Samples were scored according to immune cell infiltrate into the tumor. All tumor samples were scored by two independent blinded readers. Readers evaluated cores at 20X magnification and scored each core as either negative (≤1% of cells stained) or positive (>1% of cells stained). Agreement between readers was assessed with Cohen's kappa statistic. The scores from both readers for all available cores from each patient were averaged to generate a composite score rounded to the nearest whole number (<0.5 to 0 for negative, ≥0.5 to 1 for positive). This score was matched to the SUV_{max} for that tumor, and the SUV_{max} values of tumors that stained positive vs. negative were compared using the Wilcoxon two sample test.

Tissue Culture and Reagents

Two human cervical cancer cell lines obtained through the ATCC collection were evaluated: ME180 and SiHa. Experiments were performed on cell lines between passages 10 and 30. Mycoplasma testing was performed by the iPSC Center (ME180 and SiHa cells, 2/20/2019) at Washington University School of Medicine. All experiments were carried out under standard tissue culture conditions at 37° C and 5% CO_2, with cells maintained in IMDM media with 10% fetal bovine serum (FBS) and 0.1 mg/mL gentamycin.

Macrophage Co-Culture and Conditioned Media Experiments

Human monocytic THP-1 cells were differentiated into M0, M1, and M2 macrophages using methods outlined in the Supplemental Methods. The generation of macrophage conditioned media is also outlined in the Supplemental Methods.

In the co-culture experiments, SiHa and ME180 cells were plated onto 6 or 12 well plates, and THP-1 monocytes were differentiated into M0, M1, or M1 macrophages in 6 or 12 Transwell inserts (membrane pore size of 0.4 μm, Corning). Cells were co-cultured for 48 hrs. For the conditioned media experiments cervical cancer cells were maintained as above and directly exposed to conditioned media collected from different macrophages. Cervical cancer cells from both conditioned media and co-culture experiments were harvested after 48 hours for Western blot analysis or a glucose uptake assay.

Western Blotting

Activation of STAT3 by co-culture with macrophages was confirmed using Western blotting with primary antibodies against total STAT3 (1:1000, room temperature for 1 hour, Santa Cruz Biotech) and phosphorylated STAT3 (pSTAT3 (Tyr705), 1:2000, 4° C overnight, Cell Signaling Technology). Blots were probed with horseradish peroxidase–conjugated anti-rabbit (1:3000, Cell Signaling Technology) for 1 hour at room temperature. Blotting was also performed for actin (1:1000; Santa Cruz Biotech) at room temperature for 1 hour. The STAT3 and actin primary antibodies were both conjugated to HRP. Whenever necessary, blots were stripped by incubating membrane with restore Western blot stripping buffer (Thermo scientific) with intermittent shaking and reprobed with required antibodies. For detection, Amersham ECL select (GE Healthcare) was used according to the manufacturer's protocol. Images were acquired using Chemidoc Imaging systems (BioRad).

Fluorescent 2-DG Glucose Uptake Assay

A glucose uptake assay was performed using 2-[N-(7-nitrobenz-2-oxa-1,3-diazol-4-yl)amino]-2-deoxy-D-glucose (2-NBDG; Cayman) by flow cytometric detection of fluorescence produced by the cells. Briefly, cervical cancer cells were plated in 12 well plate and co-culture with macrophages or conditioned media collected from macrophages as described above. After 48 h of exposure, cells were trypsinized, washed in PBS and stained by 2-NBDG. For 2-NBDG uptake in the experimental settings of α-IL6, cells were exposed with α-IL6 (500 μg/ml). After 48 h of exposure, cells were washed three times with PBS to remove remaining α-IL6 from the culture media. Subsequently, cells were trypsinized, washed in PBS and stained by 2-NBDG. Flow cytometry was performed using a

MACSQuant Analyzer10 flow cytometer (Miltenyi Biotec). For each measurement, data from 10,000 single-cell events were collected using FACScan flow cytometer.

Cytokine Array Analysis

Cytokines were analyzed by human Discovery Assay using an array of 13 cytokines (Human Cytokine Array/Chemokine Array 13-Plex, Eve Technologies Corporation). For each sample, conditioned or culture media was collected from macrophages co-cultured with ME180 cells as a supernatant and processed by according to the company's specifications and requirements.

RESULTS

Patients

The cohort of patients used in the SUV_{max} analysis (cohort 1) consisted of 318 patients, the cohort of patients used for the RNAseq analysis (cohort 2) consisted of 68 patients, and the cohort used for the TMA consisted of 82 patients. All but 8 of the patients in cohort 2 were also included in cohort 1, and all but 11 of the patients in cohort 3 were also included in cohort 1. Patient characteristics are summarized in Table 1, and the overlap between the cohorts is summarized in Supplemental Figure 1S. We compared the characteristics of the patients included only in the SUV_{max} analysis with the patients included in both the SUV_{max} analysis and RNAseq analysis, and also with the patients included in both the SUV_{max} analysis and the TMA analysis. There were no significant differences between these groups in terms of age at diagnosis, FIGO stage, lymph node involvement by FDG-PET, histology, or the primary tumor SUV_{max} (Table 1).

Median follow-up was 3.2 years for cohort 1, 4.0 years for cohort 2, and 5.1 years for cohort 3. Overall survival (OS) rates at 2 and 5 years were 76.1% and 66.8%, respectively, in cohort 1; 72.5% and 56.5%, respectively, in cohort 2; and 69.5% and 56.1%, respectively, in cohort 3. Cancer-specific survival (CSS) rates at 2 and 5 years were 77.6% and 70.7%, respectively, in cohort 1; 64.7% at both 2 and 5 years in cohort 2; and 73.2% and 61.0%, respectively, in cohort 3.

Prognostic Value of SUV_{max}

Using outcome-oriented cutoff methodology, an $SUV_{max} < 11.41$ was found to be most prognostic of freedom from progression (FFP). This is similar to the SUV_{max} of 13.3 previously reported as being associated with the worst survival (7). This SUV_{max} cutoff was also prognostic of CSS, but not OS (Figure 1a–c), and was prognostic for local (cervical) recurrence and any pelvic recurrence as well (Supplemental Figure 3S). On Cox univariate analysis, SUV_{max} (≥ vs. < 11.41), FIGO stage, and lymph node involvement on PET (para-aortic vs. none) were found to be prognostic for FFP. On multivariate analysis for FFP, SUV_{max}, FIGO stage, and lymph node involvement were all significant (Table 2).

We also performed a bootstrap multivariate analysis to further determine the relative prognostic significance of SUV_{max} (≥ vs. < 11.41) in the context of other known clinical prognostic variables; namely age at diagnosis, FIGO stage, nodal involvement on pre-

treatment FDG-PET/CT, and histology. Results summarized in Supplemental Table 1 demonstrate that in 1000 random samplings from cohort 1, SUV_{max} proved to be a significant prognostic factor 63.3% of the time, FIGO stage 72.1% of the time with FIGO stage III portending a particularly poor prognosis, nodal involvement 96.5% of the time with para-aortic lymph node involvement being a powerful prognostic variable, and age and histology 12.6 and 12.0% of the time, respectively. Median hazard ratios and p-values when each variable was included in the model are shown in Supplemental Table 1.

Gene Sets Associated with High SUV_{max}

Once the association of SUV_{max} and prognosis was established, we performed a gene set enrichment analysis (GSEA) on the RNA_{seq} data to determine gene sets associated with a high SUV_{max}. The GSEA was performed treating SUV_{max} as a dichotomous variable (≥ or < 11.41). We focused on Hallmark gene sets, which represent well-defined biologic states that display coherent expression, and have been generated using a computational methodology (27). The top 3 Hallmark gene sets associated with high SUV_{max} were for inflammatory response, TNFα signaling via NF-κB, and JAK/STAT3 signaling (Figure 2). There was overlap between many of the genes in these gene sets (i.e., gene present in >1 gene set). Furthermore, many of these genes encode cytokines and chemokines associated with specific immune cell subpopulations, including cells within the myeloid lineage, and macrophages in particular (Figure 2).

Computational Prediction of Immune Cell Populations Associated with High SUV_{max}

Given the association between high SUV_{max} and inflammatory pathway genes related to myeloid cell populations, we performed a deconvolution of the bulk RNA_{seq} data using the CIBERSORT algorithm. The relative prevalence of neutrophils, monocytes, and NK cells were significantly different between the high and low SUV_{max} groups, with higher proportions of neutrophils and monocytes and lower proportions of NK cells in the high SUV_{max} group (Figure 3A). The proportion of macrophages almost met the threshold for significance ($p = 0.066$, Figure 3A). Given the number of genes related to macrophages overexpressed in the high SUV_{max} tumors in the GSEA, we also examined the predicted prevalence of macrophage subgroups, and found that a greater proportion of M2 polarized macrophages were predicted in high SUV_{max} tumors (Figure 3B).

Prevalence of Macrophages and Neutrophils in a Cervical Cancer TMA

To validate the findings from the GSEA and CIBERSORT data suggesting that high SUV_{max} is associated with inflammatory pathways and immune cells in the myeloid lineage, we performed immunohistochemistry (IHC) staining on a TMA of human cervical cancer tumors to identify immune cell subpopulations. We specifically focused on surface markers for neutrophils and macrophages. CD68 expression was used as a general marker of macrophages, with good agreement between the 2 readers (kappa = 0.69). Tumor samples with minimal/negative CD68 staining (≤1%) showed a lower average SUV_{max} than samples that were positive (>1%) for CD68 (Figure 3C). CD163 expression was used as a marker of M2 polarized macrophages. There was no significant difference in the SUV_{max} between samples that were negative for CD163 versus those that were positive (Supplemental Figure 4S). To evaluate neutrophil infiltrate, separate TMA slides were co-stained with CD66b and

neutrophil elastase; there was good agreement between readers of neutrophil staining (kappa = 0.70). There was a non-significant positive correlation between SUV_{max} and neutrophil infiltrate in the tumor microenvironment (Figure 3D).

M0 and M2 Macrophages Alter Glucose Metabolism in Human Cervical Cancer Cells through Inflammatory Signaling Pathways

To study the relationship between macrophages, glucose uptake, and JAK/STAT3 signaling, human monocytic THP-1 cells were differentiated into macrophages using phorbol 12-myristate 13-acetate (PMA), then further polarized into M1 macrophages using interferon-γ (INF-γ) and lipopolysaccharide (LPS), or M2 macrophages using IL-4 and IL-13. Human cervical cancer cells (SiHa and ME180) were then exposed to macrophage-conditioned media or were co-cultured with macrophages in transwell plates.

Glucose metabolism was measured using fluorescent 2-NBDG by flow cytometry. Exposing ME180 and SiHa cells to either M0, M1, or M2 macrophage-conditioned media, or co-culturing ME180 and SiHa cells with M0, M1, or M2 macrophages, resulted in a significant increase in 2-NBDG uptake by the cervical cancer cells. This was seen in both cell lines with all subtypes of macrophages (Figure 4A). We therefore evaluated an array of 13 pro-inflammatory cytokines and chemokines that were secreted in this transwell system (Eve Technologies). This demonstrated an increase in a wide array of cytokines secreted by macrophages. Two cytokines, IL-1β and IL-6, showed consistent increases when macrophages were co-cultured with cervical cancer cells, compared to the macrophages alone (Figure 4B). Results from 4 cytokines are not shown (INFγ, IL-2, IL-4, and IL-13) because either the signal for most conditions was too low to be detected (INFγ and IL-2), or the signal from ME180 cells alone outweighed that from the macrophages by several orders of magnitude (IL-4 and IL-13).

We further explored the impact of IL-6 on glucose metabolism in ME180 and SiHa cells. IL-6 is known to activate the JAK/STAT3 pathway, resulting in STAT3 phosphorylation. ME180 cells showed no baseline STAT3 phosphorylation, but showed STAT3 phosphorylation when cultured with macrophages or macrophage conditioned media. SiHa cells showed baseline STAT3 phosphorylation, which was unchanged or possibly slightly diminished when co-cultured with macrophages and macrophage conditioned media (Figure 4C). Treatment with neutralizing antibody to IL-6 (500 ng/ml) resulted in a decrease in STAT3 expression in SiHa cells (D), as well as a decrease in glucose uptake, as measured by 2-NBDG when either SiHa or ME180 cells were co-cultured with M2 macrophages (Figure 4E).

Finally, to connect JAK/STAT3 signaling to glucose metabolism in human tumors, we repeated the GSEA analysis, but ranking expressed genes according to STAT3 expression as opposed to SUV_{max}. The Hallmark Glycolysis pathway was significantly upregulated in tumors with high STAT3 expression (FDR q-value <0.0001, FWER p-value <0.0001).

DISCUSSION:

In this work, we have made a connection between a high SUV_{max} derived from FDG-PET, an immune infiltrate characterized by myeloid-derived cells, particularly monocytes and M2 macrophages, and inflammatory signaling pathways. As high SUV_{max} is also prognostic, this could therefore serve as an imaging biomarker to identify high-risk cancers with a specific inflammatory and immune profile, and guide use of novel targeted or immune therapies for these patients. To our knowledge, these are the first data to demonstrate a connection between tumor glucose metabolism, inflammatory signaling pathways, and immune cell infiltrate in cervical cancer.

Our data specifically suggest that a high SUV_{max} is associated with inflammatory pathways, including JAK/STAT3 and NF-κB signaling (Figure 2), both of which have previously been implicated as important signaling pathways in cervical cancer. Activated STAT3 (pSTAT3) has been shown to be a poor prognostic marker in cervical squamous cell carcinoma (28, 29). Likewise, NF-κB signaling has been implicated in cervical cancer carcinogenesis, progression, and therapeutic resistance, though the exact role of NF-κB in cervical cancer appears to be complex (30, 31). In addition, many of the genes identified in these pathways in our cohort have been shown to have prognostic significance or important biologic implications in cervical cancer, including IL-6 (32).

The inflammatory pathway gene sets associated with high SUV_{max} on the GSEA share a number of genes, particularly cytokines and chemokines linked with myeloid-derived immune cells (Figure 2). The association between SUV_{max} and myeloid derived immune cells was further supported by our CIBERSORT and IHC analyses (Figure 3). The CIBERSORT algorithm showed an association between SUV_{max} and neutrophils, monocytes, and M2 polarized macrophages, and a negative association with NK cells, and the IHC analysis of the TMA further supported the association between CD68 positive cells (i.e. monocytes and macrophages) and SUV_{max}. An association between neutrophils and SUV was not seen on the TMA, though this remains an active area of investigation (33). The negative association between SUV_{max} and NK cells seen in the CIBERSORT analysis is interesting given the known high glucose uptake of NK cells (34). It is possible that the tumor microenvironment is modulating expression of NK cell genes included in the LM22 signature used for CIBERSORT (35). This study therefore provides the important insight that the immune microenvironment and tumor glycolysis are interconnected.

We have further demonstrated a connection between glucose metabolism, macrophage infiltrate, and JAK/STAT3 signaling (Figure 4). Specifically, we have shown that co-culturing human cervical cancer cells with macrophages or growing cervical cancer cells with macrophage-conditioned media results in increased glucose uptake. Cytokine array profiling showed IL-6 and IL-1β concentrations were significantly increased in media from macrophages co-cultured with ME180 cells, compared to media from the macrophages alone, suggesting an interplay between the cervical cancer cells and the macrophages that alters expression of these factors. Co-culture with macrophages also increased STAT3 phosphorylation in ME180 cells, and treatment with neutralizing antibody to IL-6 decreased glucose uptake in SiHa and ME180 cells. Finally, we demonstrated that the Hallmark

Glycolysis gene set is significantly upregulated in human tumors with high STAT3 expression, once again utilizing GSEA analysis.

In aggregate, these data demonstrate: 1) primary tumor SUV_{max} is associated with FFP and CSS in women with cervical cancer; 2) high SUV_{max} is associated with inflammatory signaling pathways; 3) high SUV_{max} is also associated with a myeloid-derived immune cell infiltrate, particularly macrophages. We propose that the relationship between cervical cancer glucose metabolism and macrophage immune infiltrate is mediated in part by cytokines and chemokines involved in JAK/STAT3 signaling. There is some other evidence in the literature that STAT3 can impact glucose metabolism through modifying hexokinase expression, FOXO1 and HIF1α signaling, and mitochondrial metabolism, though further study is needed to establish the exact mechanism of this connection in cervical cancer (36–38). Notably, we did not establish a connection between SUV_{max} and the Hallmark Hypoxia signature in our GSEA.

The clinical implications of inflammatory pathways and immune makeup in cervical cancers is actively being investigated and elucidated. Tumor-associated macrophages have been shown to be prevalent in cervical tumors, more so than regulatory T cells, suggesting they contribute to an immunosuppressive tumor microenvironment (24, 39, 40). Tumor-associated macrophages have also been associated with poor prognosis in cervical cancers (26, 41). JAK/STAT3 is also a targetable pathway, and ruxolitinib is clinically used in blood disorders, and is under investigation in a number of cancers (NCT02713386, NCT02876302, NCT03120624) (42, 43). Our data provide a link between a pro-inflammatory but immunosuppressive microenvironment in cervical cancer, and a routinely clinically measured imaging metric, the PET-derived SUV_{max} for FDG.

This study has important limitations. We have focused on the SUV_{max} of cervical tumors treated at a single institution with a robust PET imaging program over a recent period of time (since 2006). There are a number of potential critiques regarding using SUV_{max} as a quantitative marker. In this case, our PET data were derived from several different scanners with differing performance characteristics, and the discriminating value for high versus low SUV_{max} in this study reflects this specific dataset. We have not validated the reproducibility of SUV_{max} in cervical cancer across a broad array of scanners, reconstruction methods, and different imaging centers, and it is therefore not clear how easily it could be adopted as a quantitative predictive biomarker across many institutions (44). Future studies could alternatively utilize SUV_{peak}, most typically defined as the average SUV within a small volume (e.g., 1 cm^3) within the highest uptake region of the tumor, or an SUV ratio. These have been suggested as a more robust alternative to SUV_{max} less sensitive to differences in noise, scanner resolution, and reconstruction, and both have some evidence to support their use in cervical cancer (45–47). Although it has limitations, SUV_{max} is simple to measure, is one of the of the most widely reported FDG-PET metrics in standard clinical interpretations, and we have previously reported its prognostic significance in a separate cohort of cervical cancer patients (7, 48, 49). Regardless, our data have outlined high FDG uptake as a poor prognostic factor that is correlated with the inflammatory state and immune infiltrate in cervical cancer tumors, even if our specific SUV_{max} cutoff may not hold true across a more diverse array of scanners and institutions. Because of its broad clinical availability, the

connection between FDG uptake and inflammatory and immune state could have immediate clinical and therapeutic implications.

Future work should focus on further study and characterization of the interplay between immune infiltrate and cervical cancer metabolism, and on validating our connection between high SUV_{max} for FDG and a macrophage-predominant immune infiltrate. With regard to the connection between glucose metabolism and immune infiltrate, here we have broadly established an interplay between the presence of macrophages, or macrophage-conditioned growth medium, and cervical cancer glucose metabolism. We focused on factors associated with JAK/STAT3 signaling, and IL-6 in particular, as our GSEA and cytokine array data suggested this as a potential candidate for mediating this effect. However, the interactions between macrophages and cervical cancer cells are certainly complex, and mediated by a host of other factors. We have also recently demonstrated a connection between FDG uptake, oxidative stress, and radioresistance in cervical cancer cell lines and animal models (50). Further work should explore the interplay between glucose utilization, oxidative stress and the inflammatory and immune microenvironment in primary cervical tumors.

In sum, we have demonstrated that a high SUV_{max} for FDG is prognostic of outcomes in cervical cancer, and also associated with pro-inflammatory signaling pathways and a monocytic immune infiltrate. Ultimately, SUV_{max} may potentially be used as a surrogate marker for this microenvironment to identify cancers that can be treated with therapies targeting pro-inflammatory pathways (e.g. JAK/STAT3 signaling) or therapies that aim to reverse the infiltration of tumor associated macrophages and other cells that suppress adaptive immunity.

Supplementary Material

Refer to Web version on PubMed Central for supplementary material.

ACKNOWLEDGEMENTS

We would like to thank Marina Platik and the Anatomic and Molecular Pathology Core Laboratory at Washington University in St. Louis for their assistance in staining the TMA. We would also like to acknowledge Songyang Wang, MD, PhD and Min Tan from Stephanie Markovina's laboratory for their assistance with immunohistochemistry and for supplying supplies, reagents, and expertise for investigating the JAK/STAT3 pathway.

Financial Support:

This work was supported in part by NIH R01CA181745 and the AACR Bristol Myers Squibb Mid Career Female Investigator Award to JK Schwarz.; by NIH K08CA237822 to S Markovina, by NCI K22CA237839 to J Zhang, and by ASTRO Resident Research Seed Grant 531448 and the RSNA Resident Research Grant to JM Floberg.

REFERENCES

1. Jemal A, Bray F, Center MM, Ferlay J, Ward E, Forman D. Global cancer statistics. CA Cancer J Clin. 2011;61(2):69–90. [PubMed: 21296855]
2. Eifel PJ, Winter K, Morris M, Levenback C, Grigsby PW, Cooper J, et al. Pelvic irradiation with concurrent chemotherapy versus pelvic and para-aortic irradiation for high-risk cervical cancer: an update of radiation therapy oncology group trial (RTOG) 90–01. J Clin Oncol. 2004;22(5):872–80. [PubMed: 14990643]

3. Rose PG, Ali S, Watkins E, Thigpen JT, Deppe G, Clarke-Pearson DL, et al. Long-term follow-up of a randomized trial comparing concurrent single agent cisplatin, cisplatin-based combination chemotherapy, or hydroxyurea during pelvic irradiation for locally advanced cervical cancer: a Gynecologic Oncology Group Study. J Clin Oncol. 2007;25(19):2804–10. [PubMed: 17502627]
4. Lanciano R, Calkins A, Bundy BN, Parham G, Lucci JA, Moore DH, et al. Randomized comparison of weekly cisplatin or protracted venous infusion of fluorouracil in combination with pelvic radiation in advanced cervix cancer: a gynecologic oncology group study. J Clin Oncol. 2005;23(33):8289–95. [PubMed: 16230678]
5. Tewari KS, Sill MW, Penson RT, Huang H, Ramondetta LM, Landrum LM, et al. Bevacizumab for advanced cervical cancer: final overall survival and adverse event analysis of a randomised, controlled, open-label, phase 3 trial (Gynecologic Oncology Group 240). Lancet. 2017;390(10103):1654–63. [PubMed: 28756902]
6. Schmidt AM, Imesch P, Fink D, Egger H. Indications and long-term clinical outcomes in 282 patients with pelvic exenteration for advanced or recurrent cervical cancer. Gynecol Oncol. 2012;125(3):604–9. [PubMed: 22406639]
7. Kidd EA, Siegel BA, Dehdashti F, Grigsby PW. The standardized uptake value for F-18 fluorodeoxyglucose is a sensitive predictive biomarker for cervical cancer treatment response and survival. Cancer. 2007;110(8):1738–44. [PubMed: 17786947]
8. Schwarz JK, Siegel BA, Dehdashti F, Grigsby PW. Association of posttherapy positron emission tomography with tumor response and survival in cervical carcinoma. JAMA. 2007;298(19):2289–95. [PubMed: 18029833]
9. Kidd EA, Siegel BA, Dehdashti F, Grigsby PW. Pelvic lymph node F-18 fluorodeoxyglucose uptake as a prognostic biomarker in newly diagnosed patients with locally advanced cervical cancer. Cancer. 2010;116(6):1469–75. [PubMed: 20108309]
10. Ho JC, Allen PK, Bhosale PR, Rauch GM, Fuller CD, Mohamed AS, et al. Diffusion-Weighted Magnetic Resonance Imaging as a Predictor of Outcome in Cervical Cancer After Chemoradiation. Int J Radiat Oncol Biol Phys. 2017;97(3):546–53. [PubMed: 28011045]
11. Halle C, Andersen E, Lando M, Aarnes EK, Hasvold G, Holden M, et al. Hypoxia-induced gene expression in chemoradioresistant cervical cancer revealed by dynamic contrast-enhanced MRI. Cancer Res. 2012;72(20):5285–95. [PubMed: 22890239]
12. Schwarz JK, Payton JE, Rashmi R, Xiang T, Jia Y, Huettner P, et al. Pathway-specific analysis of gene expression data identifies the PI3K/Akt pathway as a novel therapeutic target in cervical cancer. Clin Cancer Res. 2012;18(5):1464–71. [PubMed: 22235101]
13. Dyk P, Jiang N, Sun B, DeWees TA, Fowler KJ, Narra V, et al. Cervical gross tumor volume dose predicts local control using magnetic resonance imaging/diffusion-weighted imaging-guided high-dose-rate and positron emission tomography/computed tomography-guided intensity modulated radiation therapy. Int J Radiat Oncol Biol Phys. 2014;90(4):794–801. [PubMed: 25245584]
14. Network CGAR, Medicine AECo, Services AB, Hospital BC, Medicine BCo, Hope BRIoCo, et al. Integrated genomic and molecular characterization of cervical cancer. Nature. 2017;543(7645):378–84. [PubMed: 28112728]
15. Wright JD, Dehdashti F, Herzog TJ, Mutch DG, Huettner PC, Rader JS, et al. Preoperative lymph node staging of early-stage cervical carcinoma by [18F]-fluoro-2-deoxy-D-glucose-positron emission tomography. Cancer. 2005;104(11):2484–91. [PubMed: 16270319]
16. Contal C, O'Quigley J. An application of changepoint methods in studying the effect of age on survival in breast cancer. Computational Statistics & Data Analysis. 1999;30(3):253–70.
17. Dobin A, Gingeras TR. Mapping RNA-seq Reads with STAR. Curr Protoc Bioinformatics. 2015;51:11.4.1–9. [PubMed: 26334920]
18. Liao Y, Smyth GK, Shi W. featureCounts: an efficient general purpose program for assigning sequence reads to genomic features. Bioinformatics. 2014;30(7):923–30. [PubMed: 24227677]
19. Trapnell C, Williams BA, Pertea G, Mortazavi A, Kwan G, van Baren MJ, et al. Transcript assembly and quantification by RNA-Seq reveals unannotated transcripts and isoform switching during cell differentiation. Nat Biotechnol. 2010;28(5):511–5. [PubMed: 20436464]

20. White NM, Zhao SG, Zhang J, Rozycki EB, Dang HX, McFadden SD, et al. Multi-institutional Analysis Shows that Low PCAT-14 Expression Associates with Poor Outcomes in Prostate Cancer. Eur Urol. 2017;71(2):257–66. [PubMed: 27460352]
21. Subramanian A, Tamayo P, Mootha VK, Mukherjee S, Ebert BL, Gillette MA, et al. Gene set enrichment analysis: a knowledge-based approach for interpreting genome-wide expression profiles. Proc Natl Acad Sci U S A. 2005;102(43):15545–50. [PubMed: 16199517]
22. Newman AM, Liu CL, Green MR, Gentles AJ, Feng W, Xu Y, et al. Robust enumeration of cell subsets from tissue expression profiles. Nat Methods. 2015;12(5):453–7. [PubMed: 25822800]
23. Markovina S, Wang S, Henke LE, Luke CJ, Pak SC, DeWees T, et al. Serum squamous cell carcinoma antigen as an early indicator of response during therapy of cervical cancer. Br J Cancer. 2018;118(1):72–8. [PubMed: 29112685]
24. Ring KL, Yemelyanova AV, Soliman PT, Frumovitz MM, Jazaeri AA. Potential immunotherapy targets in recurrent cervical cancer. Gynecol Oncol. 2017;145(3):462–8. [PubMed: 28233576]
25. Kamper P, Bendix K, Hamilton-Dutoit S, Honoré B, Nyengaard JR, d'Amore F. Tumor-infiltrating macrophages correlate with adverse prognosis and Epstein-Barr virus status in classical Hodgkin's lymphoma. Haematologica. 2011;96(2):269–76. [PubMed: 21071500]
26. Kawachi A, Yoshida H, Kitano S, Ino Y, Kato T, Hiraoka N. Tumor-associated CD204. Cancer Sci. 2018;109(3):863–70. [PubMed: 29274107]
27. Institute B Gene Set Enrichment Analysis: MSigDB Collections 2017 [Available from: http://software.broadinstitute.org/gsea/msigdb/collections.jsp.
28. Sobti RC, Singh N, Hussain S, Suri V, Bharti AC, Das BC. Overexpression of STAT3 in HPV-mediated cervical cancer in a north Indian population. Mol Cell Biochem. 2009;330(1–2):193–9. [PubMed: 19421717]
29. Takemoto S, Ushijima K, Kawano K, Yamaguchi T, Terada A, Fujiyoshi N, et al. Expression of activated signal transducer and activator of transcription-3 predicts poor prognosis in cervical squamous-cell carcinoma. Br J Cancer. 2009;101(6):967–72. [PubMed: 19638983]
30. Tilborghs S, Corthouts J, Verhoeven Y, Arias D, Rolfo C, Trinh XB, et al. The role of Nuclear Factor-kappa B signaling in human cervical cancer. Crit Rev Oncol Hematol. 2017;120:141–50. [PubMed: 29198328]
31. DA Costa RM, Bastos MM, Medeiros R, Oliveira PA. The NFκB Signaling Pathway in Papillomavirus-induced Lesions: Friend or Foe? Anticancer Res. 2016;36(5):2073–83. [PubMed: 27127107]
32. Luan S, An Z, Bi S, Chen L, Fan J. Interleukin 6 receptor (IL-6R) was an independent prognostic factor in cervical cancer. Histol Histopathol. 2018;33(3):269–76. [PubMed: 28741286]
33. Wisdom AJ, Hong CS, Lin AJ, Xiang Y, Cooper DE, Zhang J, et al. Neutrophils promote tumor resistance to radiation therapy. Proc Natl Acad Sci U S A. 2019;116(37):18584–9. [PubMed: 31462499]
34. Chan WK, Au WY, Wong CY, Liang R, Leung AY, Kwong YL, et al. Metabolic activity measured by F-18 FDG PET in natural killer-cell lymphoma compared to aggressive B- and T-cell lymphomas. Clin Nucl Med. 2010;35(8):571–5. [PubMed: 20631501]
35. Chang WC, Li CH, Chu LH, Huang PS, Sheu BC, Huang SC. Regulatory T Cells Suppress Natural Killer Cell Immunity in Patients With Human Cervical Carcinoma. Int J Gynecol Cancer. 2016;26(1):156–62. [PubMed: 26512789]
36. Li M, Jin R, Wang W, Zhang T, Sang J, Li N, et al. STAT3 regulates glycolysis via targeting hexokinase 2 in hepatocellular carcinoma cells. Oncotarget. 2017;8(15):24777–84. [PubMed: 28445971]
37. Zheng M, Cao MX, Yu XH, Li L, Wang K, Wang SS, et al. STAT3 Promotes Invasion and Aerobic Glycolysis of Human Oral Squamous Cell Carcinoma via Inhibiting FoxO1. Front Oncol. 2019;9:1175. [PubMed: 31750256]
38. Poli V, Camporeale A. STAT3-Mediated Metabolic Reprograming in Cellular Transformation and Implications for Drug Resistance. Front Oncol. 2015;5:121. [PubMed: 26106584]
39. Piersma SJ. Immunosuppressive tumor microenvironment in cervical cancer patients. Cancer Microenviron. 2011;4(3):361–75. [PubMed: 21626415]

40. Pedraza-Brindis EJ, Sánchez-Reyes K, Hernández-Flores G, Bravo-Cuellar A, Jave-Suárez LF, Aguilar-Lemarroy A, et al. Culture supernatants of cervical cancer cells induce an M2 phenotypic profile in THP-1 macrophages. Cell Immunol. 2016;310:42–52. [PubMed: 27502363]

41. Zijlmans HJ, Fleuren GJ, Baelde HJ, Eilers PH, Kenter GG, Gorter A. The absence of CCL2 expression in cervical carcinoma is associated with increased survival and loss of heterozygosity at 17q11.2. J Pathol. 2006;208(4):507–17. [PubMed: 16435282]

42. Stover DG, Gil Del Alcazar CR, Brock J, Guo H, Overmoyer B, Balko J, et al. Phase II study of ruxolitinib, a selective JAK1/2 inhibitor, in patients with metastatic triple-negative breast cancer. NPJ Breast Cancer. 2018;4:10. [PubMed: 29761158]

43. Hurwitz HI, Uppal N, Wagner SA, Bendell JC, Beck JT, Wade SM, et al. Randomized, Double-Blind, Phase II Study of Ruxolitinib or Placebo in Combination With Capecitabine in Patients With Metastatic Pancreatic Cancer for Whom Therapy With Gemcitabine Has Failed. J Clin Oncol. 2015;33(34):4039–47. [PubMed: 26351344]

44. Velasquez LM, Boellaard R, Kollia G, Hayes W, Hoekstra OS, Lammertsma AA, et al. Repeatability of 18F-FDG PET in a multicenter phase I study of patients with advanced gastrointestinal malignancies. J Nucl Med. 2009;50(10):1646–54. [PubMed: 19759105]

45. Vanderhoek M, Perlman SB, Jeraj R. Impact of the definition of peak standardized uptake value on quantification of treatment response. J Nucl Med. 2012;53(1):4–11. [PubMed: 22213818]

46. Schernberg A, Reuze S, Orlhac F, Buvat I, Dercle L, Sun R, et al. A score combining baseline neutrophilia and primary tumor SUV. Eur J Nucl Med Mol Imaging. 2018;45(2):187–95. [PubMed: 28916879]

47. Kunos C, Radivoyevitch T, Abdul-Karim FW, Faulhaber P. 18F-fluoro-2-deoxy-D-glucose positron emission tomography standard uptake value ratio as an indicator of cervical cancer chemoradiation therapeutic response. Int J Gynecol Cancer. 2011;21(6):1117–23. [PubMed: 21792015]

48. Lodge MA, Chaudhry MA, Wahl RL. Noise considerations for PET quantification using maximum and peak standardized uptake value. J Nucl Med. 2012;53(7):1041–7. [PubMed: 22627001]

49. Wahl RL, Jacene H, Kasamon Y, Lodge MA. From RECIST to PERCIST: Evolving Considerations for PET response criteria in solid tumors. J Nucl Med. 2009;50 Suppl 1:122S–50S. [PubMed: 19403881]

50. Rashmi R, Huang X, Floberg JM, Elhammali AE, McCormick ML, Patti GJ, et al. Radioresistant Cervical Cancers Are Sensitive to Inhibition of Glycolysis and Redox Metabolism. Cancer Res. 2018;78(6):1392–403. [PubMed: 29339540]

TRANSLATIONAL RELEVANCE

^{18}F-fluorodeoxyglocose pretreatment positron emission tomography (FDG-PET) is a valuable tool for evaluating cervical cancer, and maximum standardized uptake value (SUV_{max}) is a widely clinically reported metric. Previous series have shown SUV_{max} to be prognostic. In the current study we confirm the prognostic value of SUV_{max} using prospectively collected clinical outcome data for 318 patients treated with standard of care radiotherapy. Using smaller cohorts, we identify gene signatures and immune cell populations associated with a high SUV_{max} using whole transcriptome analysis and immunohistochemistry analysis of a tissue microarray. We show high SUV_{max} is associated with inflammatory gene signatures (e.g. JAK/STAT3 signaling) and myeloid-derived immune infiltrates, particularly macrophages. We then demonstrate that co-culture of macrophages with cervical cancer cells alters tumor JAK/STAT3 signaling, and this in turn increases glucose uptake. Therefore, SUV_{max} could be used to identify cancers susceptible to therapies targeting select inflammatory pathways and infiltration by tumor permissive immune sub-populations.

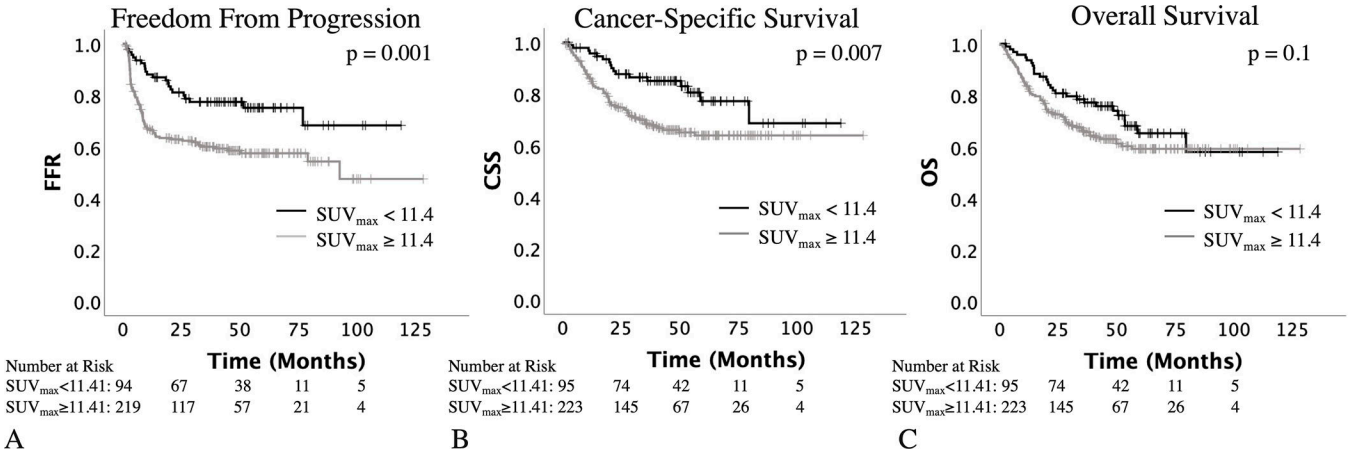

Figure 1.

Prognostic significance of SUV_{max}. An SUV_{max} cutoff of 11.4 was prognostic for freedom from progression and cause-specific survival (A and B) but not overall survival (C, p values represent results of the log-rank test).

Inflammatory Response

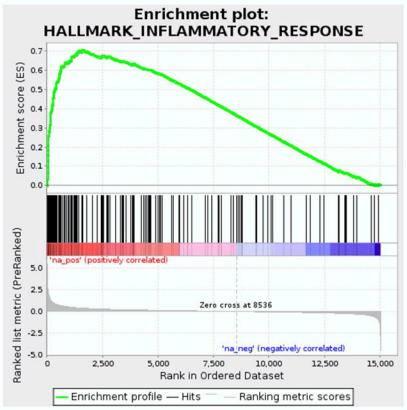

A

P < 0.0001
FDR < 0.0001
FWER < 0.0001

NF-kB Signaling

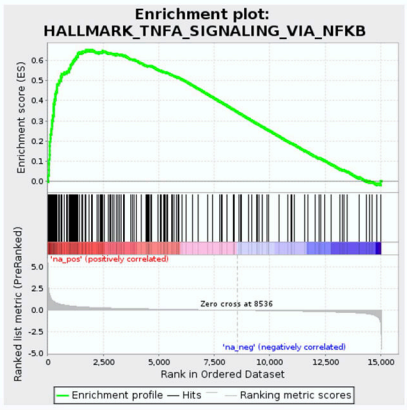

B

P < 0.0001
FDR < 0.0001
FWER < 0.0001

JAK/STAT3 Signaling

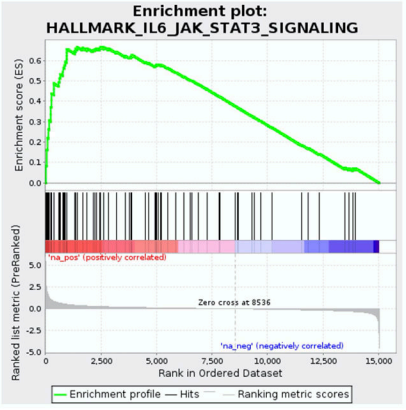

C

P < 0.0001
FDR = 0.002
FWER = 0.057

Common Genes

CCL20	Chemotactic for lymphocytes and **dendritic** cells. Dependent on JAK/STAT3 and NFKB activation
CCL2	Recruits **macrophages**, **monocytes**, **memory T-cells**, and **dendritic cells**
IL1	Produced by **macrophages**, **monocytes**, fibroblasts, and **dendritic cells**
IL6	Produced by **T-cells** and **macrophages**. Polarizes macrophages toward M2 phenotype
OLR1	Receptor for oxidized LDL on **macrophages**, endothelial, and smooth muscle cells
CXCL1	Expressed by **macrophages**, **neutrophils**, epithelial cells. Angiogenesis and tumorigenesis
CXCL3	Controls adhesion and migration of **monocytes**
CXCL2	Secreted by **macrophages**. Attracts **neutrophils** and **myeloid** derived suppressor cells
TNFSF9	Cytokine involved in antigen processing and presentation to **cytotoxic T-cells**
IL7R	Cytokine receptor expressed on naïve and **memory T-cells**
CSF3/R	Initiates differentiation of precursor cells into **granulocytes** and **macrophages**
SerpinE1	Serine protease inhibitor
CXCL10	Secreted by **monocytes**, chemoattractant for **macrophages**, **T cells**, **NK cells**, and **dendritic cells**
PDE4B	Cyclic nucleotide phosphodiesterase, regulates signal transduction
SOCS3	Negative Regulator of cytokine signaling
LIF	Activates JAK/STAT and MAPK signaling. Induces terminal differentiation of myeloid leukemic cells
F3	Tissue factor. Initiates thrombin formation

D

Figure 2.

Results of the GSEA analysis. Considering the Hallmark pathways (well-defined biologic states), the top three pathways significantly upregulated in tumors with a high SUV_{max} were Inflammatory Response (A), TNF-α signaling via NF-κB (B), and IL-6 JAK STAT3 signaling (C). All remained significant accounting for false discovery rate (FDR), and the Inflammatory Response and NF-κB gene sets also had a family-wise error rate (FWER) < 0.05, though JAK/STAT3 signaling did not. These gene sets shared a number of genes, many

of which help regulate immune cells (**bolded**), particularly myeloid-derived cells. The genes displayed were shared by at least 2 of the gene sets.

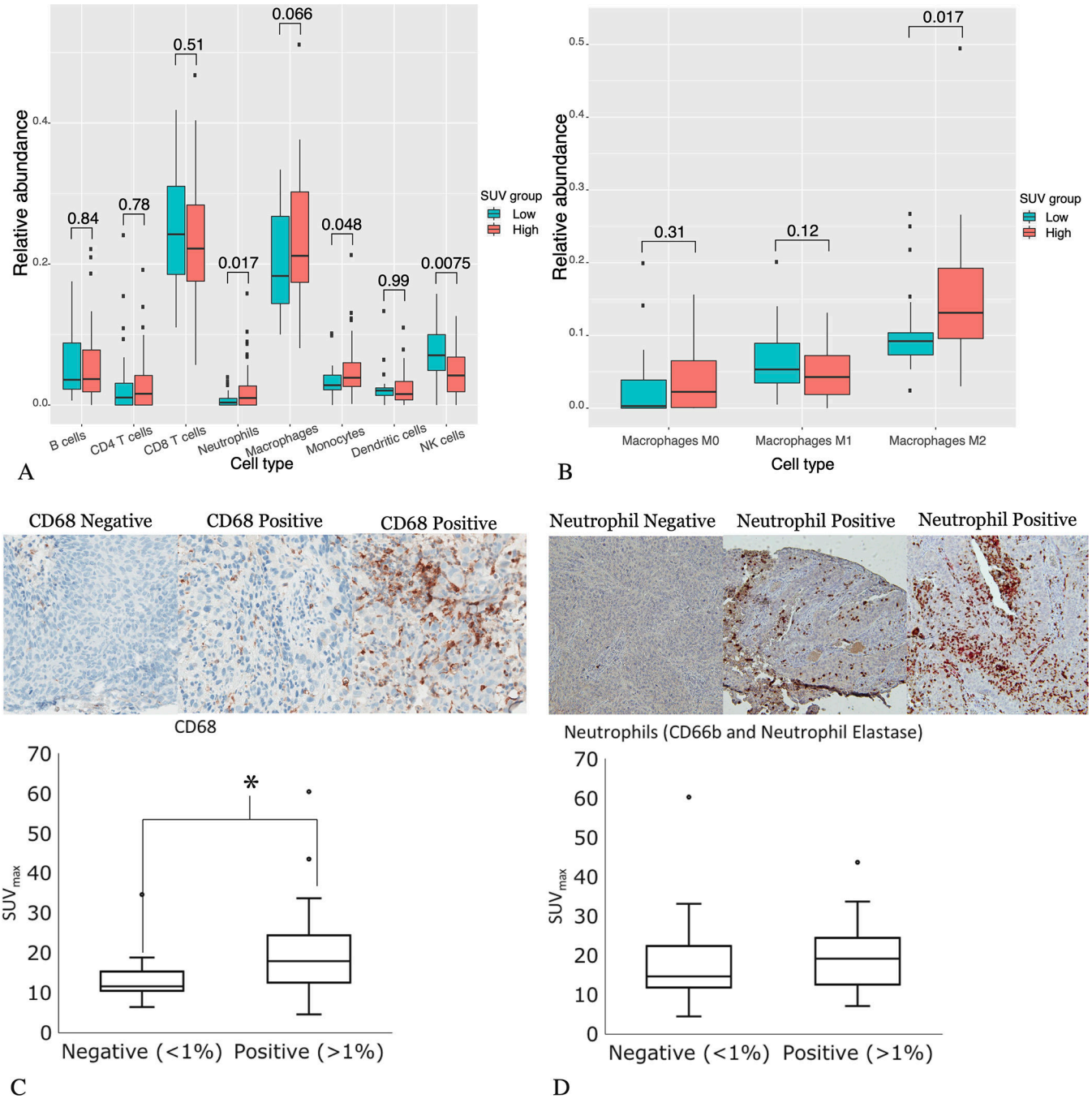

Figure 3.

Results of the CIBERSORT analysis and the tissue microarray. CIBERSORT identified neutrophils and monocytes as significantly more prevalent, and NK cells as significantly less prevalent in the high SUV_{max} tumors (A). Further sub-dividing macrophages, CIBERSORT identified M2 polarized macrophages as more prevalent in the high SUV_{max} tumors (B). We stained a TMA of human cervical cancer tumors for CD68 (a marker for macrophages) and CD66b and neutrophil elastase (markers for neutrophils). Example slides representing negative and positive staining (with a range of positive staining) are shown for both CD68

(C) and CD66b and neutrophil elastase co-staining (D). There was a significant difference in the average SUV_{max} between samples that stained positive (n = 62) for CD68 versus those that were negative (n = 14, p = 0.006 by the Wilcoxon 2-sample test), (C). There was no significant difference in the average SUV_{max} in samples that were positive (n = 38) versus negative (n = 26) for neutrophils (p = 0.24), (D).

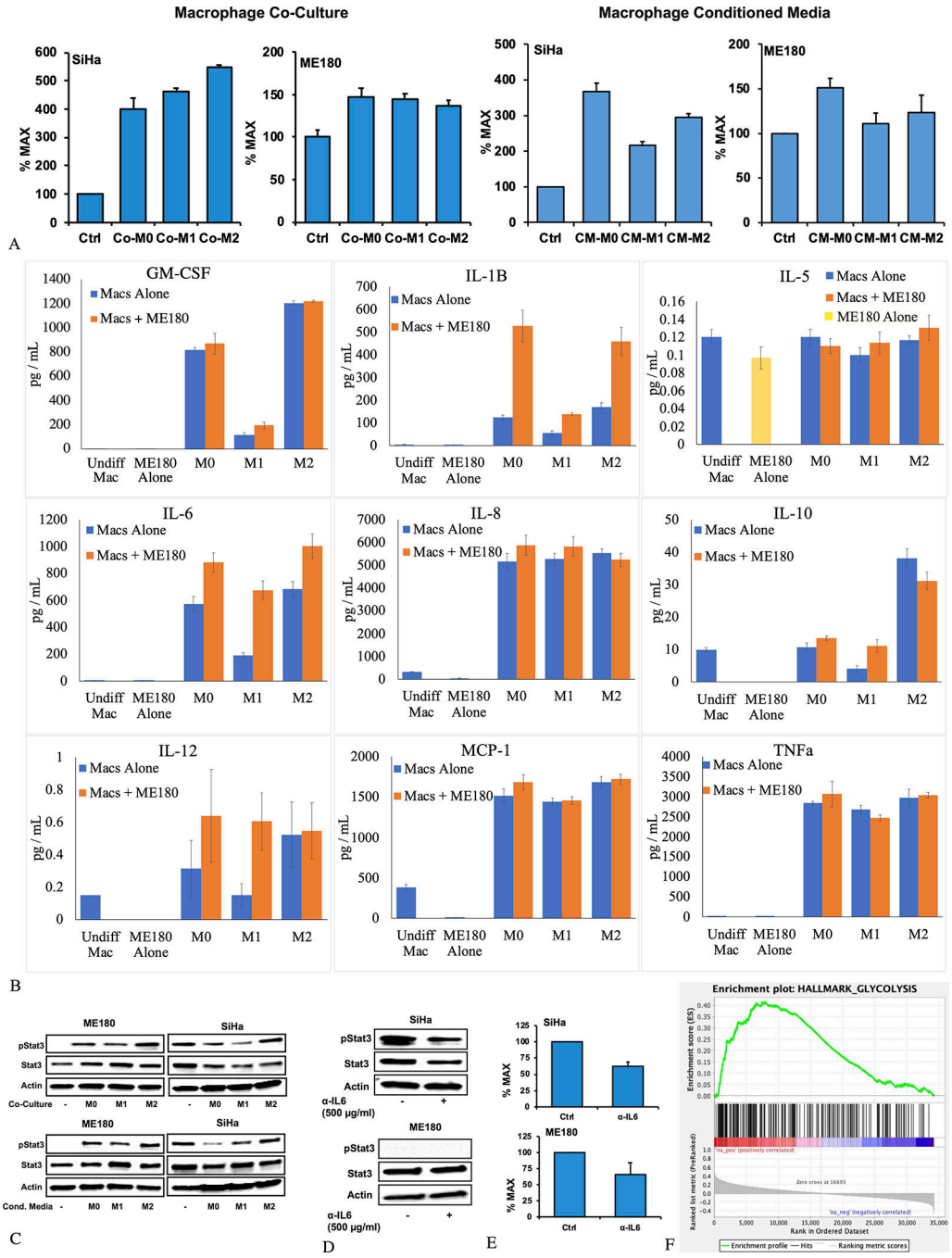

Figure 4.

Changes in glucose metabolism, cytokine and chemokine expression, and JAK/STAT3 signaling seen with co-culture of cervical cancer cells and macrophages and macrophage-conditioned media. Co-culture of macrophages with ME180 and SiHa cells, or culturing ME180 and SiHa cells with macrophage-conditioned media, results in a significant increase in 2-NBDG signal measured by flow cytometry; this is most pronounced in the SiHa cells (A). Differentiated macrophages produce a number of cytokines; co-culture with ME180 cells significantly increased expression of IL-1β and IL-6 compared to differentiated

macrophages alone (B). Co-culture with differentiated macrophages, or culturing with macrophage-conditioned media, induces STAT3 phosphorylation in ME180 cells, which have little STAT3 phosphorylation at baseline. This effect was not seen in SiHa cells, which show high baseline levels of STAT3 phosphorylation (C). SiHa cells cultured with IL-6 NAB do show reduced STAT3 phosphorylation (D). Treatment of macrophages co-cultured with cervical cancer cells with IL-6 NAB alters 2-NBDG uptake in both ME180, and SiHa cells. This effect was most pronounced with SiHa cells, and co-culture of either SiHa or ME180 cells with M2 macrophages (E). GSEA analysis showed that the Hallmark Glycolysis pathway was significantly upregulated in tumors with high STAT3 expression (F). Experiments were carried out in triplicate (n = 3) with error bars representing standard deviation.

Table 1:

Patient characteristics of the 3 study cohorts (SUV_{max}, RNA_{seq}, and TMA). A substantial number of the patients in the RNA_{seq} and TMA cohorts were also included in the SUV_{max} analysis. The p-values shown represent comparisons between patients included in both the RNA_{seq} and SUV_{max} analysis versus patients included only in the SUV_{max} analysis to determine if the RNA_{seq} subgroup was biasing the overall cohort (using the Fisher's exact or Wilcoxon tests as appropriate). The same was done for the TMA subgroup.

	SUV Cohort	RNAseq Cohort	p-value	TMA Cohort	p-value
All patients	318	68 (57 in SUV cohort)		82 (67 in SUV cohort)	
Age at Diagnosis			0.42		0.94
Median (Range)	50 (23–92)	53 (25–81)		52 (25–92)	
FIGO Stage (%)			0.52		0.26
I	125 (39.3 %)	20 (29.4%)		29 (35.4%)	
II	119 (37.4%)	25 (36.8%)		28 (34.1%)	
III	69 (21.7%)	21 (30.9%)		22 (26.8%)	
IV	5 (1.6%)	2 (2.9%)		3 (3.7%)	
Lymph Node Involvement (%)			0.08		0.82
None	146 (45.9%)	33 (48.5%)		40 (58.8%)	
Pelvic	122 (38.4%)	21 (30.9%)		27 (32.9%)	
Para-aortic/supraclavicular	50 (15.7%)	14 (20.6%)		15 (18.3%)	
Histology			0.85		0.86
Squamous	256 (80.5%)	55 (80.9%)		56 (80.5%)	
Non-squamous	62 (19.5%)	13 (19.1%)		16 (19.5%)	
Adenocarcinoma	42 (13.2%)	9 (13.2%)		10 (12.2%)	
Small cell	8 (2.5%)	2 (2.9%)		2 (2.4%)	
Adenosquamous	4 (1.3%)	2 (2.9%)		1 (1.2%)	
Other	8 (2.5%)	0		3 (3.7%)	
SUVmax			0.65		0.19
Mean (Range)	14.6 (2.9 – 60.3)	17.0 (3.4–53.6)		15.4 (3.77–60.3)	

Table 2.

Cox Univariate and multivariate analysis for freedom from progression

	Univariate		Multivariate	
Variable	**HR (95% CI)**	**p**	**HR (95% CI)**	**p**
SUV_{max} (≥ vs < 11.41)	2.20 (1.37–3.54)	0.001	1.73 (1.06–2.81)	0.03
FIGO Stage				
II vs. I	1.28 (0.80–2.06)	0.30	1.07 (0.66–1.73)	0.79
III vs. I	2.83 (1.76–4.55)	<0.0001	1.98 (1.20–3.27)	0.008
IV vs. I	4.75 (1.67–13.5)	0.003	2.30 (0.77–6.88)	0.14
III/IV vs. I/II	2.59 (1.76–3.82)	<0.0001	1.89 (1.26–2.86)	0.002
Lymph Nodes				
Pelvic vs. none	1.30 (0.83–2.03)	0.25	1.27 (0.81–2.00)	0.30
Para-aortic vs. none	3.93 (2.47–6.24)	<0.0001	3.03 (1.88–4.88)	<0.0001
Age	1.00 (0.98–1.01)	0.54		
Histology (Squamous vs. Non-squamous)	0.99 (0.61–1.59)	0.96		